Journal of Magnetic Resonance **139,** 26–34 (1999)
Article ID jmre.1999.1748, available online at http://www.idealibrary.com on IDEAL®

# An Integrated Head Immobilization System and High-Performance RF Coil for fMRI of Visual Paradigms at 1.5 T

Keith R. Thulborn and Gary X. Shen

*Department of Radiology, MR Research Center, Presbyterian University Hospital, University of Pittsburgh Medical Center, Pittsburgh, Pennsylvania 15123*

Received August 26, 1998; revised January 8, 1999

**A flexible quadrature radiofrequency coil that maximizes the signal-to-noise ratio over the field of view of the human brain has been integrated into a head immobilization and visor system for fMRI at 1.5 T. Head motion is reduced by the visor that incorporates a head clamp and a simple visual sighting system that provides feedback on head position. This system is demonstrated in serial images by correction of deliberate head motions. The sensitivity at the cortical surface of fMRI using blood oxygenation level dependent contrast is increased significantly above that of the commercial rigid volume RF coil under the same acquisition conditions. This improved performance is demonstrated using visual activation and eye movement paradigms.** © 1999 Academic Press

*Key Words:* **fMRI; coil; immobilization; wide field of view; surface coil.**

## INTRODUCTION

The small signal changes resulting from the hemodynamic response to neuronal activity that are detected in fMRI[1] using blood oxygenation level dependent (BOLD) contrast are of the order of 1–3% at 1.5 T (*1*). This contrast mechanism is based on the oxygenation state dependence of the magnetic properties of blood (*2, 3*). Studies at higher magnetic fields have demonstrated more robust results but such scanners remain uncommon (*4–12*). Several strategies have been integrated to improve the performance at 1.5 T to provide greater access to fMRI data from more generally available clinical scanners. Surface radiofrequency (RF) coils provide improved signal-to-noise ratio (SNR) by restricting the field-of-view (FOV). A rigid volume RF coil provides a wide FOV albeit at a lower SNR. We have fabricated a flexible array excitation/reception RF coil that uses quadrature detection and maximizes the filling factor over the whole brain to improve the SNR over a wide FOV. Head motion is the main source of excessive signal variation even in cooperative subjects. Rather than using a bite bar or thermoplastic mask that would be unsuitable for clinical studies, a head clamp has been designed to tighten the flexible RF coil around the calvarium. The visor not only restricts extraneous visual stimuli but has a sighting mechanism to provide visual feedback as to head position. This clamp is made of acoustical dampening materials to decrease the background auditory noise.

The presentation of visual stimuli has been done in a number of ways including goggles directly over the eyes (*13*) to rear-projection screens positioned on the foot of the patient table (*14*) or mounted within the bore of the magnet (*15*). Visual paradigms achieve maximum eye movement when the screen is closest to the eyes. We have used a visor that allows the supine subject to view visual stimuli on a thin rear-projection screen via an angled mirror. Results from this integrated package are presented for fMRI paradigms using visual stimulation with and without eye movement.

## RESULTS

A head restraining device, known as the head clamp and visor, was constructed from flexible multilayered orthotic sound damping foam and sound damping loaded silicon rubber materials (Fig. 1). The visor incorporates a mirror and rear-projection screen that is independent of the clamp and hinges back for subject entry. With appropriate foam cushioning to avoid pressure points on the ear lobes, the clamp tightens around the calvarium to provide firm support without discomfort for up to 1 h. A flexible surface coil is mounted within the body of the head clamp which mounts directly onto the commercial coil mounting system of the patient table of the scanner. This mounting system is normally used for holding bilateral temporomandibular joint surface coils in clinical practice but provides the mounting for the visor in the current configuration.

The effectiveness of the clamp to restrain in-plane axial head motion was evaluated during the fMRI studies for the two paradigms of visual stimulation with centrally fixated checkerboard and visually guided saccades. When using the clamp, no in-plane motion could be detected for cooperative subjects by visual inspection of axial images displayed in an animation loop. In-plane translational and rotational motions, estimated

[1] Abbreviations used: BOLD, blood oxygenation level dependent; EPI, echo-planar imaging; fMRI, functional magnetic resonance imaging; FOV, field of view; MRI, magnetic resonance imaging; NEX, number of excitations; RF, radiofrequency; SNR, signal to noise ratio; TE, time to echo; TR, repetition time.



1090-7807/99 $30.00
Copyright © 1999 by Academic Press
All rights of reproduction in any form reserved.

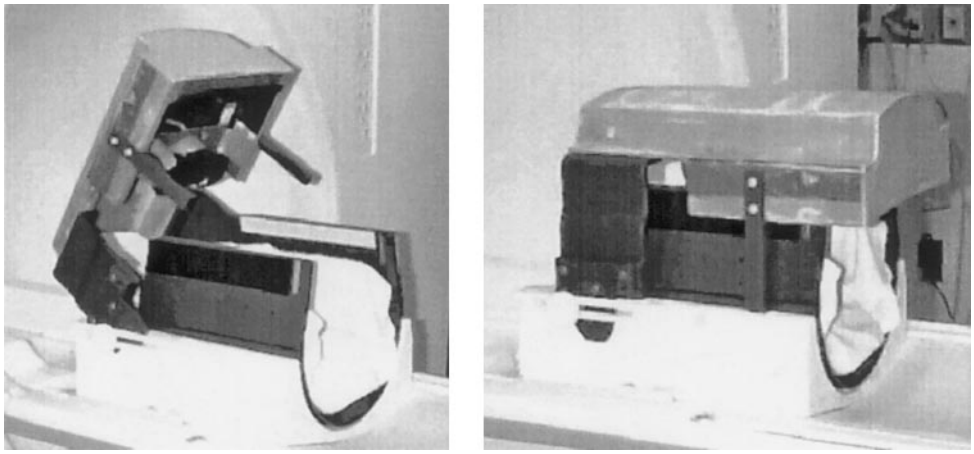

**FIG. 1.** The flexible coil–clamp–visor assembly with the visor in the open (left) and closed (right) positions showing the easy access for subject positioning. The visor restricts stray light and allows all screen adjustments to be made outside the magnet. The head clamp remains in position on the commercial table mounting assembly. Padding enclosed in a slip cover over the RF coil provides comfort and maintains hygiene between subjects.

from image registration software, were always less than 1 mm (<30% of the voxel dimension) and 0.5 degrees, respectively, over time intervals of 10 min used for the fMRI studies. The effectiveness of the sighting system in the visor to correct for flexion–extension out-of-plane motion is demonstrated in Fig. 2. The signal intensity of a single voxel changes significantly (~50%) at each requested head motion and returns to its original value (standard deviation of baseline signal intensity of 2%) as the head is repositioned (Fig. 2a). Such motion is evident in the subtraction image (Fig. 2b) generated from an image before head motion and at peak displacement. However, the subject is able to bring his head back into alignment to produce the original signal intensity to minimize edge artifact on the subtraction image (Fig. 2c).

The performance of the RF coil over the FOV of a human brain is demonstrated for gradient-echo and spin-echo echo-planar images in Figs. 3a and 3b, respectively. As the tuning of the coil is dependent on the coupling to the sample and hence the tightness of the clamp, tuning and matching of the coil to the appropriate resonance frequency and resistance with the subject in position optimizes performance. Adequate RF penetration over the volume of the brain is shown for both sequences by the uniformity of signal intensity from the image at the cerebral vertex superiorly to the level of the cerebellum inferiorly. The signal loss from the frontal lobes and orbits is due to the sensitivity of echo-planar imaging to magnetic susceptibility effects from the paranasal sinuses. As expected, this is more prominent on the gradient-echo images.

Figure 4 compares the variation of the signal-to-noise ratio along profiles across the field of view for the flexible coil and the commercial quadrature head volume coil. The data indicate that a SNR improvement of up to 50–75% is realized over the cortex of the temporal and parietal lobes and up to 20–40% is obtained in the superficial occipital cortex of the brain using the flexible coil. A small reduction (~10%) in signal intensity occurs in the anterior aspect of the frontal lobes due to the decreased B1 field in this area.

Given the improvement in SNR and the increased control of

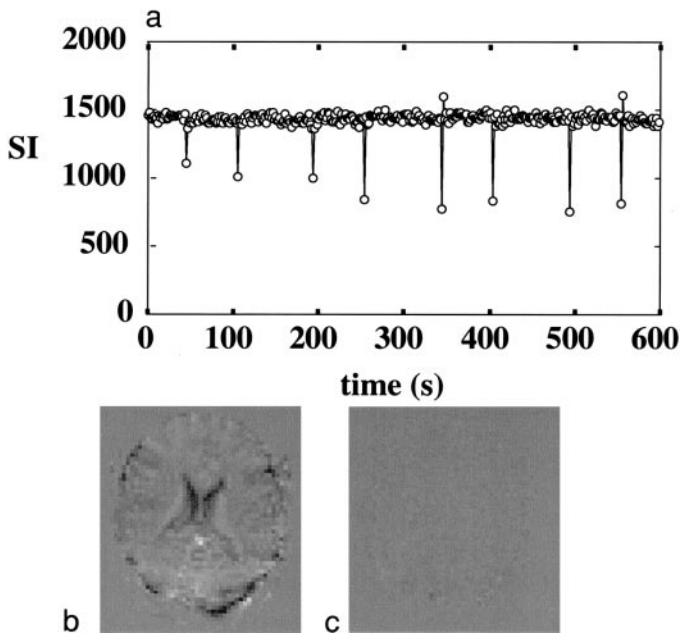


**FIG. 2.** Assessment of the visor sighting system to allow cooperative subjects to reposition their heads in the original position after out-of-plane motion occurs. (a) Time course of signal intensity in a voxel on a high-contrast edge showing the large changes in signal intensity associated with eight separate discrete flexion and extension displacements of the head with return to starting location as assessed by the visor sighting system. The signal intensity returns to normal after each movement. (b) Representative subtraction of an image prior to motion from the image at peak displacement. The expected edge enhancement is clearly evident. (c) Representative subtraction of images prior to and after a head motion. Minimal edge effects are present, indicating that the head was returned to its original position. Signal intensities of (b) and (c) are on the same scale.

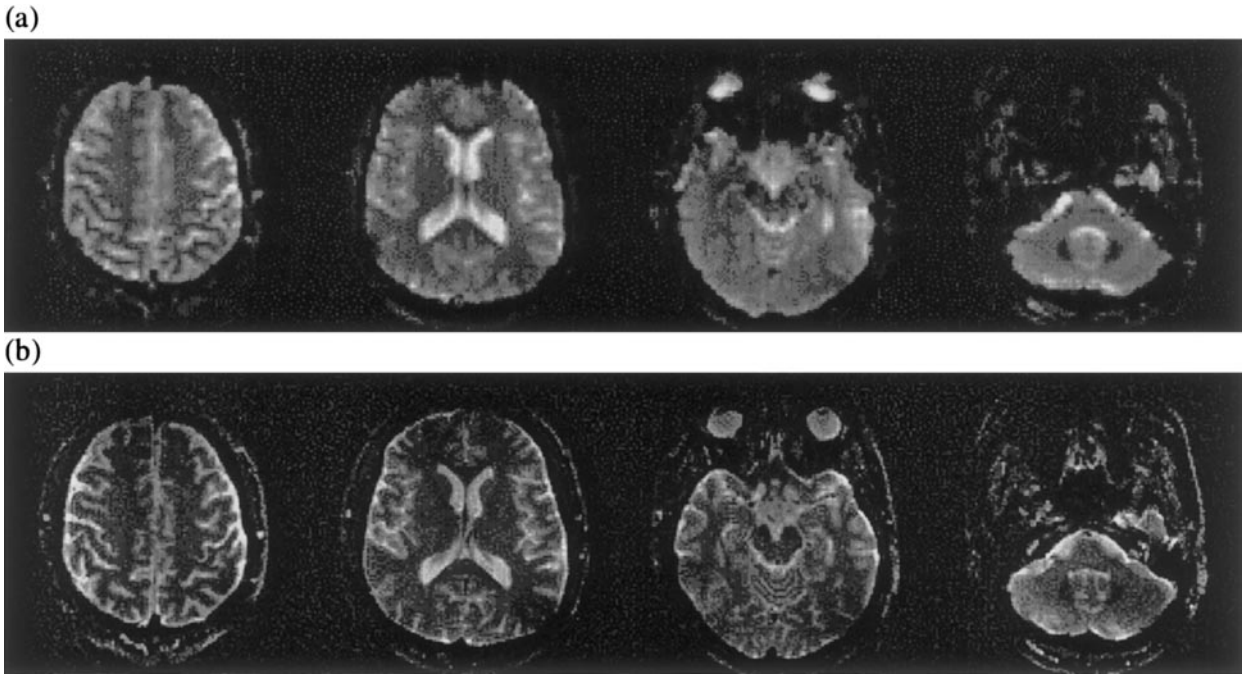


**FIG. 3.** Echo-planar images at 1.5 T acquired using the flexible quadrature coil. Magnetic susceptibility artifacts are evident from the frontal paranasal sinuses. There is some peripheral signal loss at the 5 and 7 o'clock positions from imperfection of the loop overlaps at this position. (a) Gradient-echo, echo-planar images acquired at standard resolution ($3.1 \times 3.1 \times 5.0$ mm$^3$) using flip angle = 90°, TR = 6000 ms, TE = 50 ms, and NEX = 1; and (b) spin-echo, echo-planar images acquired at high resolution ($1.6 \times 1.6 \times 3.0$ $mm^3$) using TR = 10,000 ms, TE = 71 ms, and NEX = 1.

both in-plane and out-of-plane head motions achieved by the flexible coil and clamp–visor system, fMRI experiments were performed for comparison to the commercial head coil. The visual activation with the checkerboard paradigm is a well-established paradigm and requires only central fixation. The results in Fig. 5 comparing left and right hemifield activation are equivalent to results obtained with a surface coil although the field of view covers the entire brain. The magnitudes of the change in signal intensity, measured from the 15 most significant voxels ($t > 12$), were $2.5 \pm 1$ and $3.9 \pm 1.7$% for the left and right visual cortex, respectively. Such changes are those reported elsewhere for 1.5 T. The eye movement paradigm may be expected to have increased head motion due to the movement of the eyes being coupled to head motion. This motion was not observed with the head clamp–visor system. This paradigm activates a widely distributed network which is evident in Fig. 6. The negative activations associated with the temporal lobes bilaterally are in the area of auditory cortex. This suggests that the rest condition of central fixation is an active listening condition that is less active when attention switches to the eye movement task. The activation of the frontal eye fields along the precentral sulcus is not as robust as that in the temporal, occipital, and parietal lobes, probably reflecting the reduced sensitivity over the frontal lobes evident in Fig. 4. By comparison, equivalent studies (not shown) performed with the commercial head coil on the same subjects under identical circumstances in the same imaging session produced much less robust activation as judged by volume of activation at a given $t$-statistic threshold. At a threshold of $t > 3.5$, no activation was detected in the brain with the commercial coil. The magnitude of the signal change in primary visual cortex (V1/V2) for the most significant 15 voxels ($t > 6.6$) for this paradigm was $1.3 \pm 0.5$% for the correctly tuned flexible coil.

## DISCUSSION

The routine application of fMRI has been challenging because of the small signal changes of BOLD contrast at 1.5 T. The stability of the scanner and the cooperation of the subject are vital to the success of these experiments. Many experiments have used surface coils to achieve the necessary SNR to produce results but at the cost of a markedly restricted FOV. As many cognitive processes are widely distributed over the brain, surface coils would require the integration of results from many experiments. Higher field strength magnets provide the necessary SNR to achieve whole brain imaging as well as very high spatial resolution (*13, 16*). As this technology is costly, an alternative solution was sought through the optimization of the instrumentation described in this report.

The largest source of signal intensity variation that produces technical failures in fMRI is head motion. Many algorithms have been developed to correct for head motion in postprocessing (*17, 18*). However, minimization of motion during

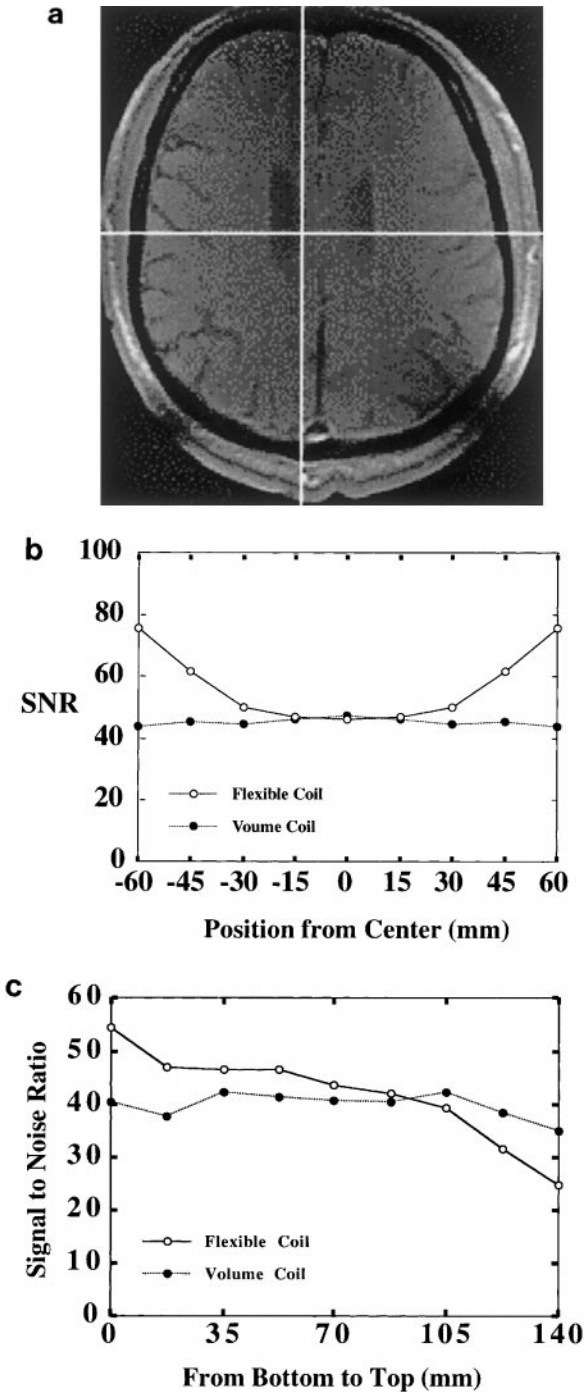


**FIG. 4.** (a) Reference image showing the position of the lateral left–right and anterior–posterior profiles of the signal to noise ratio shown in (b) and (c). Signal intensity profiles of the flexible coil (○) and commercial birdcage head coil (●) are shown in the (b) left–right direction and (c) anterior–posterior direction.

acquisition should be encouraged. The clamp provides sensitive proprioceptive feedback to the subject with minimal head motion so that the subject is aware if his head moves. The visor sighting system also provides sensitive visual feedback for the cooperative subject so that if the head does move, it can be returned to the original position immediately. This minimizes lost images and the considerable amount of time and computational resources taken in postprocessing to perform image reregistration.

Although the visual feedback system is a cognitive task in itself, it is a constant load over the experiment. The realignment system does not interfere with activation maps of paradigms in which central fixation is maintained throughout the paradigm as it becomes a constant across conditions. In a paradigm in which the eyes are not fixated (visually guided saccades) in all conditions, the visual alignment system is not used continuously but head position can be verified at the transitions between conditions in less than a second. This minimizes its effects on the analysis of the task under investigation. Our experience is that if interference occurs, it is below the reproducibility level of the activation maps derived with *t* tests.

Echo-planar imaging produces an acoustically unfavorable environment for studies of acoustical stimuli (*19, 20*). The use of acoustical dampening materials has reduced, although not eliminated, this concern. The clear deactivation in the auditory cortex shown in Fig. 6 attests to the need to choose the rest condition carefully to avoid attention shifting due to scanner noise.

## CONCLUSIONS

The current equipment allows whole brain fMRI at 1.5 T. This is suitable for mapping studies as used clinically for language mapping in presurgical planning for epilepsy (*9, 21*). However care must be taken when applying more sophisticated analyses in which quantitative results are sought (*22, 23*) as the sensitivity over the FOV is not uniform. This limitation also applies to surface coils with smaller FOV. Given the lack of acceptable activation maps with the commercial head coil under the same abbreviated paradigms, the current equipment fills an important gap between the surface coil and the volume coils for fMRI applications covering the entire human brain at 1.5 T.

## EXPERIMENTAL

### *(a) Visor with Biofeedback of Head Position*

In addition to minimizing head movement, the interpretation of fMRI data from visual stimuli requires undistorted visual stimuli and elimination of stray light. The visor, a separate component from the head clamp described below, accomplishes these goals by using a thin rear-projection screen mounted on the front end of a fiberglass form molded to the circular curvature of the bore of the magnet. This shape maximizes the size of the screen within the curved surface and avoids the lights along the top of the patient tube. A single

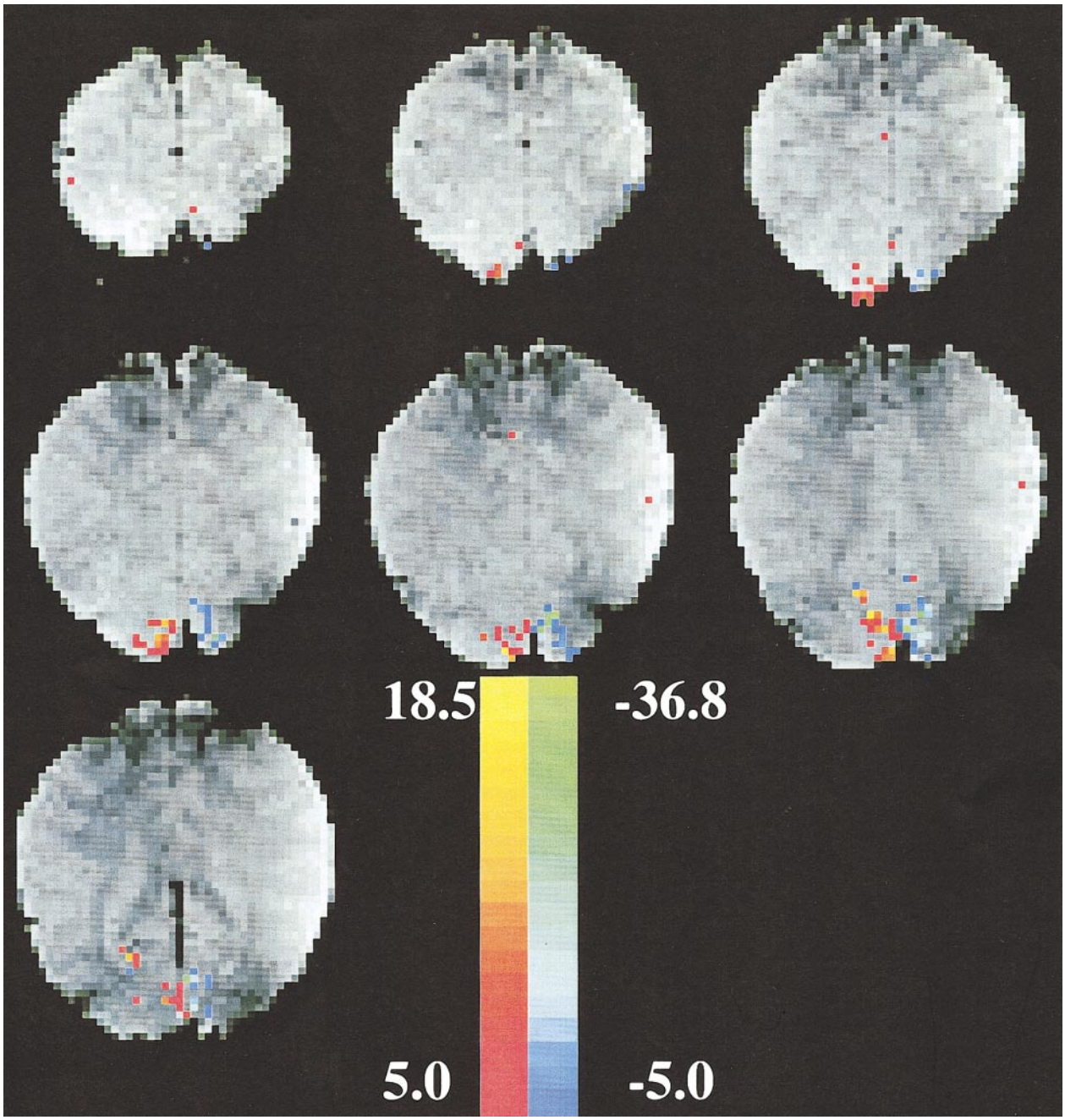


**FIG. 5.** Activation map for comparison of right and left hemifield visual activations superimposed over one of the acquired gradient-echo, echo-planar images showing robust activation in the primary visual cortex. The left and right occipital cortices show opposite activations by design of the paradigm and analysis. Although the activation is limited to the visual cortex, the entire brain is visualized. The color scale refers to the *t* values for the positive and negative tails of the *t* test used to detect the activation. The smaller positive and negative values are the thresholds for each tail. The acquisition parameters were TR = 1500 ms, TE = 50 ms, number of slices = 7, matrix = 128 × 64, FOV = 40 × 20 $cm^2$, slice thickness = 5 mm, and gap = 1 mm in the oblique axial plane.

angled large acrylic mirror (McMaster-Carr Supply Co., Dayton, NJ) is used to view the entire screen from the supine position (Fig. 7a). Visual stimuli such as sentences for reading are presented by appropriate top–bottom and left–right reversals at the computer and projector. A horizontal thread is stretched across the visor perpendicular to the light path between the mirror and the screen thereby bisecting the screen horizontally (Fig. 7b). A spot placed on the center of the screen is adjusted to be in alignment with the subject's center of view and the thread. This sighting system is readily and rapidly adjusted by the MR technologist for different subjects by manually moving the spot marked on a sticky transparent

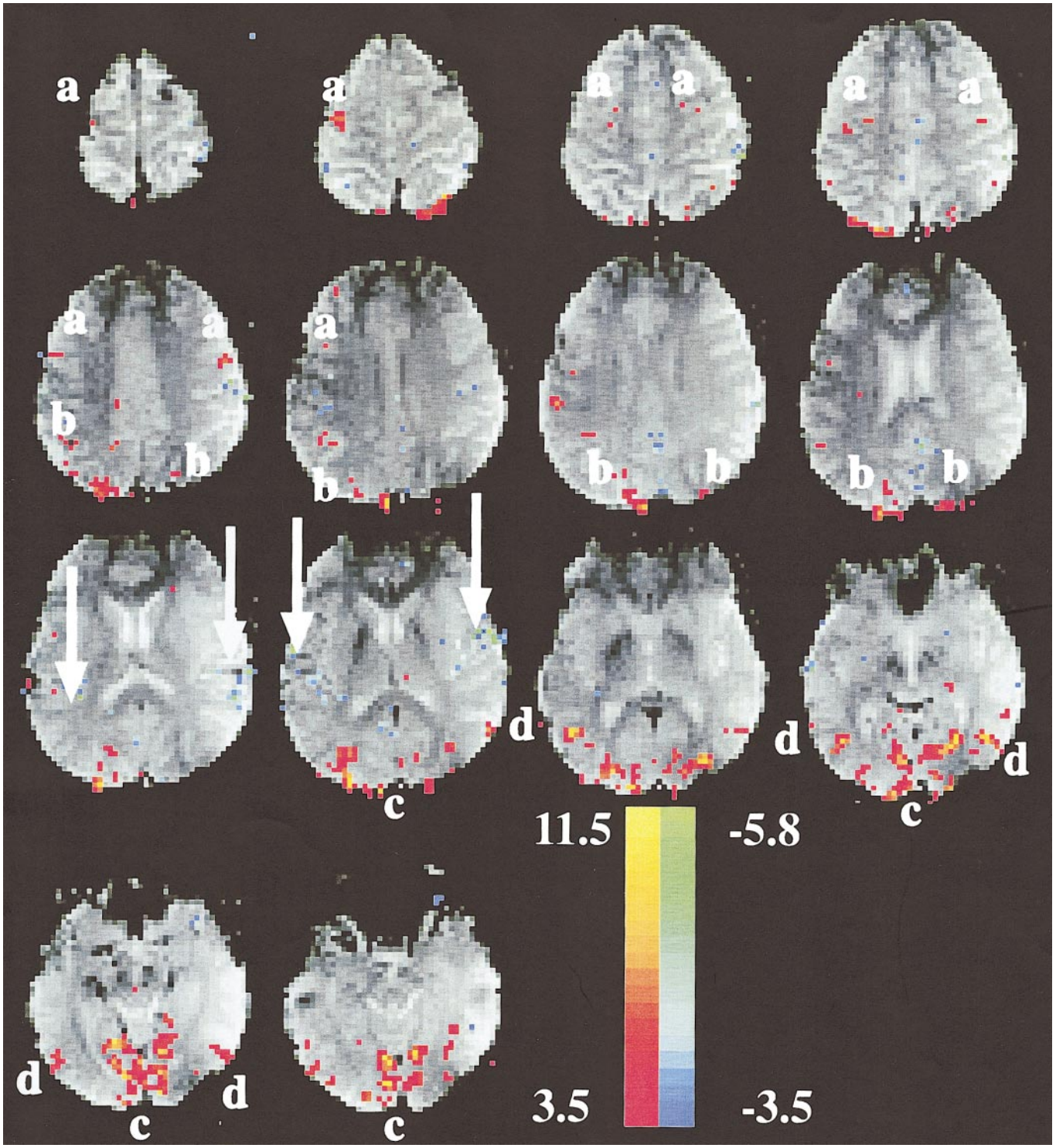


**FIG. 6.** Activation map for visually guided saccades at a *t* threshold of 3.5 superimposed over the acquired gradient-echo, echo-planar images showing robust activations in the frontal, parietal, and occipital lobes as well as deactivations in the temporal lobes (vertical white arrows). The wide field of view demonstrates the widely distributed activation due to this paradigm. Areas of activation include frontal eye fields (a), intraparietal sulci (b), primary visual cortex (c and also shown in Fig. 5) and associative visual cortex (d). Such results were not achieved under the same conditions with the commercial head coil. The color scale refers to the *t* values for the positive and negative tails of the *t* test used to detect the activation. The smaller positive and negative values are the thresholds for each tail. The acquisition parameters were TR = 3000 ms, TE = 50 ms, number of slices = 14, matrix = 128 × 64, FOV = 40 × 20 $cm^2$, slice thickness = 5 mm, and gap = 1 mm in the axial plane.

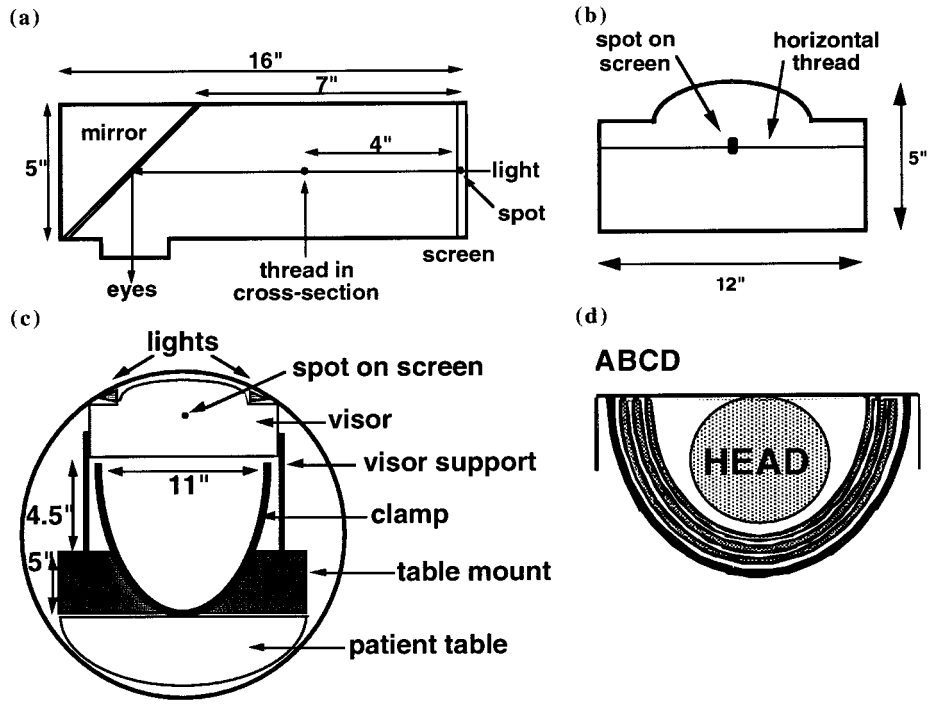


**FIG. 7.** Schematic diagram of the visor showing (a) side elevation with angled mirror, rear-projection screen, fiberglass housing, and the light path from the projector; (b) end elevation from the inside (subject's view) showing the contouring of the screen to the shape of the bore of the magnet with lights, the spot on the screen, and the horizontal thread aligned through the spot; and (c) front elevation of the magnet bore with the visor–clamp–table mount in place in the magnet. The patient table is in the lower portion of the bore. The diameter of the bore is 55 cm. Other dimensions are as shown. (d) A schematic diagram of the concentric layered cross-section of the head clamp with a head in position is shown with the different layers: (A) semi-rigid othotic material (0.5 in. thick); (B) silicon rubber (0.25 in. thick); (C) Teflon sheet (0.03 in. thick) covering the flexible circuit board coil and silicone rubber protecting the capacitors; and (D) thin foam rubber pad with exchangeable pillow slip and a cushioning pad (0.25 in. thick). The whole structure is flexible and can be narrowed by shortening the Velcro strap that extends across the open diameter at the top of the structure.

plastic tape up and down following the verbal directions of the subject until alignment is achieved with the subject in a comfortable position. This sighting system provides a visual frame of reference to ensure that if head motion does occur, as in swallowing, the head can be returned to the original position. The use of the horizontal thread avoids parallax errors from stereoscopic vision. The visor reduces flexion and extension of the head whereas the head clamp reduces side-to-side motion in the cooperative subject. The configuration of these two components in the magnet is shown in Fig. 7c.

*(b) Head Motion Restraining Device*

The multilayered clamp (Fig. 7d) incorporates the flexible printed circuit board RF coil (described below) between the inner and outer structures. The inner wall of the clamp consists of two parts: (i) cushioning pad (0.25 in. thick, ACOR Orthopedic Inc., Cleveland, OH) made from three different density orthotic foam layers that provides acoustical dampening and a pillow for the subject; and (ii) a Teflon sheet (0.03 in. thick, Small Parts Inc., Miami Lakes, FL) with a dielectric rating of greater than 60,000 V to ensure subject isolation from the RF coil. The outer structure consists of three parts: (i) sound damping loaded silicone rubber (0.25 in. thick, McMaster-Carr Supply Co.) to protect the RF coil and electronic components; (ii) semi-rigid sound damping orthotic foam (0.5 in. thick, ACOR Orthopedic Inc.) to support the coil; and (iii) Velcro straps for closure (Fig. 7d). The total of six layers reduces sound transmitted pneumatically and conducted by bone from vibrations through the patient table while providing stable head support. Ear plugs (30 dB) are still used routinely to further attenuate background sound. The flexibility of the clamp and coil allows optimum use with different head sizes. After the supine subject is positioned with his/her head within the flexible RF coil supported by the clamp, the sides of the clamp are tightened by means of a Velcro strap.

*(c) Flexible Quadrature Transmit and Receive Surface Coil*

To maximize SNR by matching the filling factor to the FOV for whole brain imaging, a EPI-compatible, flexible, quadrature surface coil was constructed to fit within the head clamp described above. This symmetric coil consists of three loops (two $4.5 \times 6.0$ in. loops and one $5.5 \times 5.5$ in. loop) made of flexible printed circuit board (Compunetix Inc., Monroeville, PA). Such board material is reliable, both electrically and

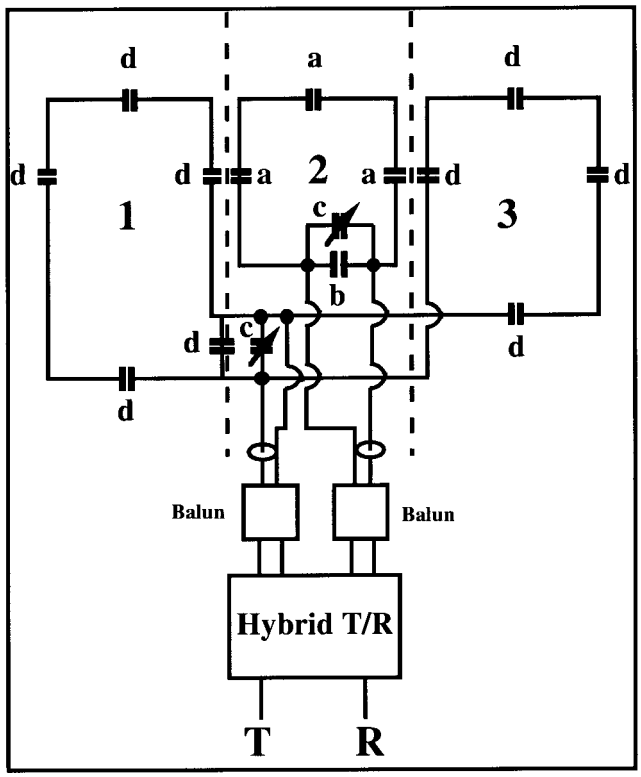


**FIG. 8.** Schematic diagram of the circuit for the flexible head coil operated in quadrature excitation/reception mode. The B1 field created by the Helmholtz pair (coils labeled 1 and 2) is perpendicular to the B1 field created by surface coil 2. The hybrid T/R switch and baluns are shown without details as they are described elsewhere (*16*). The two side loops (*1, 3*) are folded perpendicular to the central loop (*2*), as marked by the dashed lines. The capacitances are a = 56 pF, b = 22 pF, c = 2–40 pF, and d = 82 pF.

mechanically, with 2000 V of dielectric strength and 50,000 cycles of flexing life. An additional Teflon sheet (1/32 in. thick, Small Parts Inc.) with dielectric strength higher than 60,000 V further electrically isolates the subject from the RF coil. The schematic diagram of the circuit is shown in Fig. 8. The design of the hybrid transmitter/receiver switch and baluns have been described elsewhere (*24*). The coils have distributed fixed capacitance to reduce electrical losses. Variable nonmagnetic trim capacitors (Voltronics Corp., Denville, NJ) are used for matching and tuning the circuits to the required frequency.

### *(d) Imaging Protocol*

All MR imaging was performed on a 1.5-T whole body scanner (55-cm clear bore magnet, Signa, General Electric Medical Systems, Milwaukee, WI) equipped with resonant gradient, echo-planar imaging (EPI) (Advanced NMR Systems, Inc., Wilmington, MA) and data handling capabilities designed for fMRI as previously described (*7, 9*). Human subjects ($n = 6$) were healthy volunteers who provided written consent as approved by the institutional review board. Compatibility with echo-planar imaging was investigated with both spin-echo and gradient-echo EPI of human brain. Variation in SNR across the FOV was measured to assess sensitivity distribution. The acquisition parameters for gradient-echo echo-planar imaging were TR = 6000 ms, TE = 50 ms, FOV = 40 × 20, voxel size = 3.1 × 3.1 × 5.0 $mm^3$, slice thickness/gap = 5/1 mm, and number of slices = 9. The acquisition parameters for spin-echo, echo-planar imaging were TR = 10,000 ms, TE = 71 ms, FOV = 40 × 20, two-shot mosaic (*25*), slice thickness/gap = 3/1 mm, and number of slices = 9, giving a voxel size = 1.6 × 1.6 × 3.0 $mm^3$.

To demonstrate the use of the sighting system within the visor, a series of 600 gradient-echo, echo-planar images was acquired with flexible coil–visor system. On command from the operator at intervals during the acquisition, the subject quickly and maximally flexed her head and then returned to the original head position as judged by the sighting system. The subtraction of the images acquired before and after the discrete head movements were compared to subtractions of images before and during each head displacement.

Two visual paradigms were used to test the head restraint device. The flashing (8 Hz) alternating hemifield, black and white checkerboard paradigm was used to measure SNR and percentage of signal change performance of the flexible coil and the commercial quadrature birdcage head coil (General Electric Medical Systems). The paradigm compared central fixation (30 s, rest condition) to right or left hemifield flashing checkerboard (30 s, active condition) for five cycles of each hemifield stimulation. The visually guided saccade task was used to investigate sensitivity of activation over a more widely distributed activation pattern (*26*). This paradigm used blocks of central fixation (30 s, rest condition) alternating with periods of saccades to a spot of light appearing randomly at six fixed locations along the horizontal meridian subtending 26° of viewing angle (30 s, active condition).

As there is no universally accepted approach to the analysis of fMRI data, a conservative approach was chosen (*27*). Image data from both paradigms were analyzed using custom-designed software in which condition 1 (rest) was compared to condition 2 (active) via a paired two-tailed Student *t* test (*28*). For the flashing checkerboard, conditions 1 and 2 were left and right hemifield stimulation, respectively. For the visually guided saccade paradigm, conditions 1 and 2 were central fixation and saccades to unpredictable targets, respectively. No correction was required for head motion but in-plane head motion was estimated using a published algorithm for measuring such motion (*29*). Although cardiac and respiratory data were acquired during imaging, no physiological corrections were applied to the results presented (*30*).

## ACKNOWLEDGMENTS

The authors acknowledge financial support from PHS P01 NS35494, the Whitaker Foundation, PHS RO1 HL45176, PHS RO1 CA63661, the Center for the Neural Basis of Cognition, and General Electric Medical Systems. The authors thank Claudine Martin for assistance in acquisition and analysis of the fMRI data.

## REFERENCES


1. K. K. Kwong, J. W. Belliveau, D. A. Chesler, I. E. Goldberg, R. M. Weisskoff, B. P. Poncelet, D. N. Kennedy, B. E. Hoppel, M. S. Cohen, R. Turner, H-M. Cheng, T. J. Brady, and B. R. Rosen, Dynamic magnetic resonance imaging of human brain activity during primary sensory stimulation, *Proc. Natl. Acad. Sci. USA* **89,** 5675–5679 (1992).
2. S. Ogawa, T. M. Lee, A. S. Nayak, and P. Glynn, Oxygenation-sensitive contrast in magnetic resonance image of rodent brain at high fields, *Magn. Reson. Med.* **14,** 68–78 (1990).
3. K. R. Thulborn, J. C. Waterton, P. M. Mathews, and G. K. Radda, Oxygenation dependence of transverse relaxation time of water protons in whole blood at high field, *Biochim. Biophys. Acta* **714,** 265–270 (1982).
4. S. Ogawa, D. W. Tank, R. S. Menon, J. M. Ellermann, S.-G. Kim, H. Merkle, and K. Ugurbil, Intrinsic signal changes accompanying sensory stimulation: Functional brain mapping using MRI. *Proc. Natl. Acad. Sci. USA* **89,** 5951–5955 (1992).
5. R. Turner, P. Jezzard, H. Wen, K. K. Kwong, D. L. Bihan, T. Zeffiro, and R. S. Balaban, Functional mapping of the human visual cortex at 4 and 1.5 Tesla using deoxygenation contrast EPI. *Magn. Reson. Med.* **29,** 277–279 (1993).
6. P. A. Bandettini, E. C. Wong, A. Jesmanowicz, R. Prost, R. W. Cox, R. S. Hinks, J. S. Hyde, MRI of human brain activation at 0.5 T, 1.5 T and 3 T: Comparisons of ΔR2* and functional contrast to noise ratio, *in* "Proceedings, Society of Magnetic Resonance, 2nd Annual Meeting, San Francisco," p. 434 (1994).
7. K. R. Thulborn, F. E. Boada, S. Y. Chang, D. Davis, J. S. Gillen, D. C. Noll, G. X. Shen, S. L. Talagala, and X. J. Zhou, Proton, sodium and functional MRI and proton MRS at 1.5 and 3.0 Tesla, *in* "Proceedings, ISMRM, 3rd Annual Meeting, Nice, France," p. 306 (1995).
8. K. R. Thulborn, J. S. Gillen, B. McCurtain, C. Betancourt, and J. A. Sweeney, Functional magnetic resonance imaging of the human brain. *Bull. Magn. Reson.* **18,** 37–42 (1996).
9. K. R. Thulborn, J. Voyvodic, S. Chang, M. Strojwas, and J. A. Sweeney, New approaches to cognitive function by high field functional MRI, *in* "Current Progress in Functional Brain Mapping: Science and Applications" (T. Yuasa, J. W. Prichard, and S. Ogawa, Eds.), pp. 15–23, Nishimura/Smith-Gordon, Niigata/London (1998).
10. K. R. Thulborn, S. L. Talagala, S. Y. Chang, T. Tasciyan, B. McCurtain, and J. A. Sweeney, Sensitivity advantage for fMRI at 3.0 Tesla over 1.5 Tesla, *in* "Proceedings, ISMRM, 4th Annual Meeting, New York," p. 1827 (1996).
11. R. S. Menon, S. Ogawa, X. Hu, J. P. Strupp, P. Anderson, and K. Ugurbil, BOLD based functional MRI at 4 Tesla includes a capillary bed contribution: Echo-planar imaging correlates with previous optical imaging using intrinsic signals, *Magn. Reson. Med.* **33,** 453–459 (1995).
12. J. S. Gati, R. S. Menon, K. Ugurbil, and B. K. Rutt, Experimental determination of the BOLD field strength dependence in vessels and tissue. *Magn. Reson. Med.* **38,** 296–302 (1997).
13. R. S. Menon, S. Ogawa, and K. Ugurbil, Mapping ocular dominance columns in human V1 using fMRI. *NeuroImage* **3**(3), S357 (1996).
14. S-G. Kim, W. Ritcher, and K. Urgurbil, Limitations of temporal resolution in functional MRI. *Magn. Reson. Med.* **37,** 631–636 (1997).
15. R. B. H. Tootell, J. B. Reppas, A. M. Dale, R. B. Look, M. I. Sereno, R. Malach, T. J. Brady, and B. R. Rosen, Visual motion aftereffect in human cortical area MT revealed by functional magnetic resonance imaging. *Nature* **375,** 139–141 (1995).
16. K. R. Thulborn, S. Y. Chang, G. X. Shen, and J. T. Voyvodic, High resolution echo-planar fMRI of human visual cortex at 3.0 tesla. *NMR Biomed.* **10,** 183–190 (1997).
17. R. Woods, J. Mazziotta, and S. Cherry, MRI-PET registration with automated algorithm. *J. Comput. Assist. Tomogr.* **17,** 536–546 (1993).
18. K. J. Friston, S. Williams, R. Howard, R. S. J. Frackowiak, and R. Turner, Movement-related effects in fMRI time-series, *Magn. Reson. Med.* **35,** 346–355 (1996).
19. J. R. Binder, S. M. Rao, T. A. Hammeke, F. Z. Yetkin, A. Jesmanowicz, P. A. Bandettini, E. C. Wong, L. D. Estowski, M. D. Goldstein, V. M. Haughton, and J. S. Hyde, Functional magnetic resonance imaging of human auditory cortex. *Ann. Neurol.* **35,** 662–672 (1994).
20. C. M. Wessinger, M. H. Buonocore, C. L. Kussmaul, and G. R. Mangun, Tonotopy in human auditory cortex examined with functional magnetic resonance imaging. *Human Brain Mapping* **5,** 18–25 (1997).
21. K. R. Thulborn, S. Uttecht, C. Betancourt, S. L. Talagala, F. E. Boada, and G. X. Shen, A functional, physiological and metabolic toolbox for clinical magnetic resonance imaging: Integration of acquisition and analysis strategies. *Int. J. Imaging Syst. Technol.* **8,** 572–581 (1997).
22. M. A. Just, P. A. Carpenter, T. A. Keller, W. F. Eddy, and K. R. Thulborn, Brain activation modulated by sentence comprehension. *Science* **274,** 114–116 (1996).
23. M. A. Just, P. A. Carpenter, T. Keller, and K. R. Thulborn, Movies of the brain: Imaging a sequence of cognitive processes, *NeuroImage* **3**(3), S250.
24. G. X. Shen, F. E. Boada, and K. R. Thulborn, Dual-Frequency, dual-quadrature, birdcage RF coil design with identical B1 pattern for sodium and proton imaging of the human brain at 1.5 T. *Magn. Reson. Med.* **38,** 717–725 (1997).
25. M. Cohen, and R. Weisskoff, Ultra-fast imaging. *Magn. Reson. Med.* **9,** 1–37 (1991).
26. B. Luna, K. R. Thulborn, M. H. Strojwas, B. J. McCurtain, R. A. Berman, C. R. Genovese, and J. A. Sweeney, Dorsal cortical regions subserving visually-guided saccades in humans: A fMRI study. *Cerebral Cortex* **8,** 40–47 (1998).
27. C. Genovese, Why functional MRI needs statistics: Questions, models and inferences, *Comput. Sci. Stat.* **27,** 187–191 (1996).
28. K. R. Thulborn, D. Davis, P. Erb, M. Strojwas, and J. A. Sweeney, Clinical fMRI: Implementation and experience. *NeuroImage* **4,** S101–S107 (1996).
29. W. F. Eddy, M. Fitzgerald, C. R. Genovese, A. Mockus, and D. C. Noll, Functional image analysis software—computational olio, *in* "Proceedings in Computational Statistics" (A. Prat, Ed.), Vol. 12, pp. 39–49, Physica-Verlag, Heidelberg (1996).
30. T. H. Le, and X. Hu, Retrospective estimation and correction of physiological artifacts in fMRI by direct extraction of physiological activity from MR data. *Magn. Reson. Med.* **35,** 290–298 (1996).